

Acoustic Imaging using Multi-Beam Laser Radar

D.C. Jones and K.D. Ridley

QinetiQ, Malvern Technology Centre, St Andrews Road,
Malvern, Worcestershire, WR14 3PS, UK

Abstract

It is shown theoretically that synthetic acoustic images can be formed by cross correlation of laser radar echoes acquired from a scattering medium such as air or water. An array of virtual microphones is projected into the medium and the array is steered in processing to build up 2 or 3-dimensional representations of the scene. Antenna gain varies with the number of elements and angular resolution is determined by the size of the array. System noise is determined by the laser speckle coherence time, which depends on relative motion of the scattering particles.

Introduction

Detection of objects using conventional electro-magnetic imaging can suffer from a number of limitations including: attenuation, scattering and distortion of the radiation in propagating from the object to the receiver. Attenuation and scattering is often problematic for long range detection in poor weather conditions, and is a severe limitation in the underwater environment restricting detection ranges to just 10s of metres. A further limitation is the need for a direct line of sight between source and receiver.

This paper investigates the feasibility of a hybrid electro-magnetic-acoustic detection technique. Objects are detected by their acoustic emissions which may propagate over longer distances in adverse conditions. The acoustic disturbances are probed by laser radar at multiple locations near the sensor by harnessing backscatter from naturally occurring particles within the environment. Synthetic images are then constructed by processing the acquired data. The technique benefits from a virtual imaging aperture that could be 100s of meters across in air or 10s of meters in water. The aperture can be offset to allow detection beyond line-of-sight.

Concept

The concept is introduced with a simplified two dimensional depiction as shown in Figure 1.

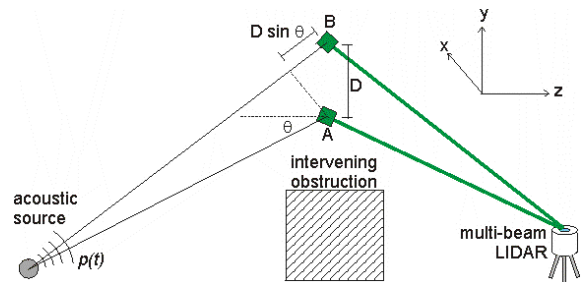


Figure 1 Two-dimensional representation of LIDAR geometry

An acoustic pressure wave $p(t)$ emitted by the object propagates to two regions of detection, A and B, with a difference in arrival times of $\tau = D \sin \theta / v_s$ where D is the baseline aperture, θ the propagation angle and v_s is the speed of sound. The detected signals are processed in the receiver to form the cross correlation $\rho(\Delta t) \propto \langle p_A(t) p_B(t - \Delta t) \rangle$, where the angled brackets indicate an average over time. This metric gives a peak proportional to $\langle p^2 \rangle$ when Δt is tuned to match τ and a small value $\langle p(t) p(t + \tau - \Delta t) \rangle$ otherwise. The system constitutes an *electronically steered coherently phased*

virtual antenna array, with the selection of Δt determining the angle of peak gain according to $\theta = \sin^{-1}(\Delta t v_s / D)$. Note that for reasons of clarity Figure 1 shows only two dimensions and two beam paths. The concept extends to location in three dimensions by adding one or more additional beams with components perpendicular to the first two.

Acoustic-induced phase shifts

The pressure wave is detected using phase sensitive laser radar of the type commonly used in laser vibrometry and Doppler wind LIDAR. A number of single frequency laser beams are transmitted to probe the disturbances at multiple points in space simultaneously. Displacement of the scattering particles induces a phase shift in the backscattered light which is detected in a heterodyne receiver. Consider a spectral component in the pressure wave with angular frequency ω_s :-

$$p = p_0 \cos(\omega_s t) \quad (1)$$

This gives a longitudinal particle displacement of

$$u = \frac{p}{Z\omega_s} = \frac{p_0 \cos(\omega_s t)}{Z\omega_s} \quad (2)$$

where Z is the acoustic impedance [1]. The optical phase detected by the heterodyne receiver is given by

$$\phi = 2u \cos(\theta)k + \phi_n \quad (3)$$

where $k = 2\pi n / \lambda$ is the propagation constant of the light, n is the refractive index, λ the laser wavelength and θ is the angle between the acoustic and optical beams. The factor 2 occurs because the light makes a double-pass from the laser to the array element and back to the detector. The term ϕ_n is a noise component due to laser speckle arising from the random distribution of scattering particles within the medium. ϕ_n will fluctuate in time due to

relative and bulk motion of the particles. Differentiating (3) gives the phase derivative

$$\begin{aligned} \dot{\phi} &= 2\dot{u} \cos(\theta)k + \dot{\phi}_n \\ &= \frac{2kp_0 \cos(\theta)}{Z} \sin(\omega_s t) + \dot{\phi}_n \end{aligned} \quad (4)$$

The volume of sound, L_p , is commonly defined in terms of the ratio of sound pressure level to a reference value, p_{ref} , in decibel (dB)

$$L_p = 10 \log \left(\frac{p_{rms}}{p_{ref}} \right)^2 = 20 \log \left(\frac{p_{rms}}{p_{ref}} \right) \quad (5)$$

where $p_{rms} = \sqrt{\langle p^2 \rangle}$. Using (4) and (5), the phase derivative can be written in terms of sound volume as

$$\dot{\phi}_{rms} = \frac{2k \cos(\theta) p_{ref}}{Z} 10^{L_p/20} + \dot{\phi}_n \quad (6)$$

Figure 2 shows a plot of the phase derivative as a function of sound pressure level for both air and water environments. For the case of air the assumed parameters are a laser wavelength of 1.5 μm (for eye safety) an impedance of 413 Pa s/m and a reference pressure of 20 μPa . For water the parameters are a laser wavelength of 532nm (close to the peak transmission through water), an impedance of 1.48 MPa s/m and a reference pressure of 1 μPa .

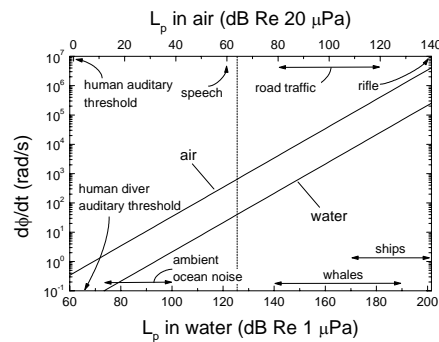


Figure 2 Calculated phase shifts induced in air and water environments as a function of sound pressure level

Note that the x axes for air and water are offset by 61.5 dB to allow like for like comparisons between air and water environments [2]. The offset is due to the different reference pressures used and the substantially different acoustic impedances of the two media.

The vertical offset between the two calculated curves is a factor of 16, i.e. acoustic induced phase shifts are a factor 16 times higher in air than water for a given acoustic intensity in Wm^{-2} .

Synthetic imaging

Synthetic images of the acoustic scene can be formed by combining recorded phase time series from multiple beams using the following metric

$$\Psi(\Delta t_1, \Delta t_2 \dots \Delta t_N) = \left\langle \left(\sum_i^N \dot{\phi}_i(t + \Delta t_i) \right)^2 \right\rangle \quad (7)$$

Here $\dot{\phi}_i$ is the phase derivative recorded in the i th array element, N is the total number of array elements, and Δt_i is the delay introduced in processing to steer the array. If noise contributions are neglected, (7) becomes

$$\Psi(\Delta t_{ij}) = \frac{4k^2 p_{rms}^2}{Z^2} \sum_i^N \sum_j^N c_i c_j \rho(\Delta t_{ij} - \tau_{ij}) \quad (8)$$

where $\Delta t_{ij} = \Delta t_i - \Delta t_j$, $\tau_{ij} = \tau_i - \tau_j$, $c_i = \cos(\theta_i)$ and

$$\rho(\tau) = \frac{\langle p(t)p(t+\tau) \rangle}{\langle p(t)p(t) \rangle} \quad (9)$$

Here $\rho(\tau)$ is the autocorrelation function of the acoustic source (allowing for any modifications due to the filtration in the signal processing chain). It can be calculated from the acoustic power spectrum via the Wiener-Khintchine theorem [3]. For the case of a Gaussian acoustic power spectrum then

$$\rho(\tau) = \cos(\omega_{s0}\tau) \exp\left(-\frac{\sigma_\omega^2 \tau^2}{2}\right) \quad (10)$$

where ω_{s0} is the centre frequency σ_ω is the spectral width at the $1/e^2$ power point. For a top-hat acoustic spectrum (i.e. *white noise* viewed through a rectangular filter)

$$\rho(\tau) = \cos(\omega_{s0}\tau) \text{sinc}\left(\frac{\Delta\omega\tau}{2}\right) \quad (11)$$

where $\Delta\omega$ is the full spectral width.

Clearly, from (8) steering the array onto the target (maximising Ψ) requires selecting the time offsets in processing such that

$$\Delta t_{ij} = \tau_{ij} \quad (12)$$

The time delays can be calculated from geometry. For example, to generate a 2-D image focused on infinity the delays are calculated in terms of two orthogonal angles of view; in alt-azimuth coordinates let θ_x represent azimuth (referenced to the minus z axis in Figure 1) and θ_y altitude.

By trigonometry it can be shown that

$$\Delta t_i = \frac{\sin \theta_x \cos \theta_y x_i + \sin \theta_y y_i + \cos \theta_x \cos \theta_y z_i}{v_s} \quad (13)$$

where (x_i, y_i, z_i) are the spatial coordinates of the array element. An identical expression holds for τ_{ij} with (θ_x, θ_y) representing the target direction.

The characteristics of the synthetic image are illustrated first using a simple planar rectangular geometry with 4 elements as shown in Figure 3. The aperture of the array is taken as 10x10m, the distance from the laser transceiver is 20m, the centre acoustic frequency is 500Hz, the spectral width is 500Hz, the speed of sound 1500m/s (appropriate for water) and the number of beams is 4. The image of a point source comprises a central peak with side spurs. These spurs can be understood by considering that for some combinations of angles the acoustic signals are correlated amongst rows of detectors but uncorrelated across columns and vice versa.

Figure 4 (LHS) is a repeat of Figure 3 but with a narrow acoustic bandwidth. In this case there are multiple side-lobes around the central peak. The side-lobes appear whenever the time offsets between array elements are integer numbers of the acoustic period. The number of side-lobes can be reduced by increasing the number of beams as shown in the right hand plot of Figure 4 for the case of 4x4 beams.

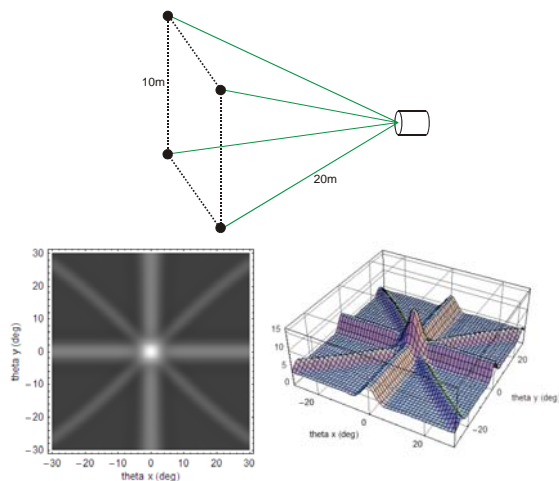


Figure 3 Example of a rectangular planar sensor array (top) with synthetic image of a broad-band source (bottom)

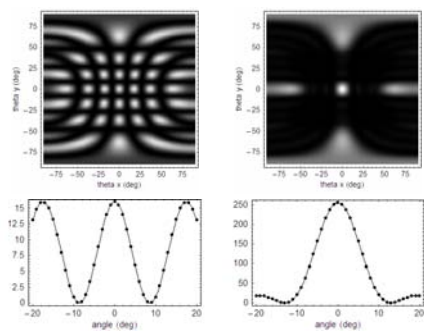


Figure 4 Side-lobe artefacts with a narrow-band source. LHS corresponds a 2x2 array of sensing elements while RHS corresponds to a 4x4 array. Cross sections compare the synthetic image points with Fraunhofer diffraction theory.

It is interesting to compare the synthetic image obtained from this virtual receiver array to that which would be formed by an

optical wave incident on a real detector sitting behind an aperture mask. In the case of a regular array of N slits, the far-field Fraunhofer diffraction pattern has a well known form:-

$$I(\theta) \propto \left(\frac{\sin(N\alpha)}{\sin(\alpha)} \right)^2 \quad (14)$$

where $\alpha = \pi D \sin(\theta)/(N-1)\lambda$ [3]. This function is plotted as the solid line in Figure 4 and shows precise agreement with the calculated synthetic image (circular points). Therefore the synthesised acoustic image is the same as would be formed by diffraction in a real detector comprising a lens behind a pinhole aperture mask with the apertures co-located with the virtual microphones.

By using range-gating techniques (and with sufficient backscatter levels) it would be possible to make measurements at multiple positions along the axis of each beam as shown in Figure 5. Adding more range bins along the beam only has a minor influence on the width of the central peak. The main benefits are in side-lobe suppression, increased array gain, and increased contrast between the peak against the spurs and incoherent background.

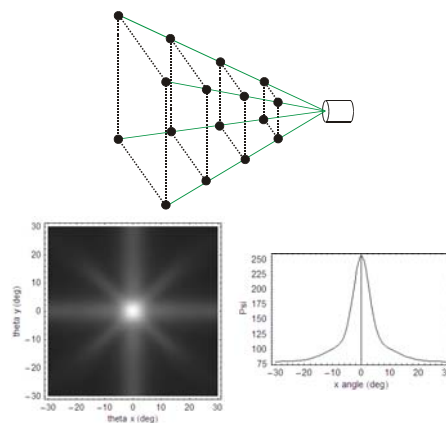


Figure 5 Volume 4-beam array (top) with synthetic image (below).

With appropriate selections of time offset values Δt_{ij} in (7), it is possible to focus the antenna at a finite distance. In Figure 6 the

focus setting is varied for three different target ranges. The calculated curves show that the synthetic image has a large depth of field.

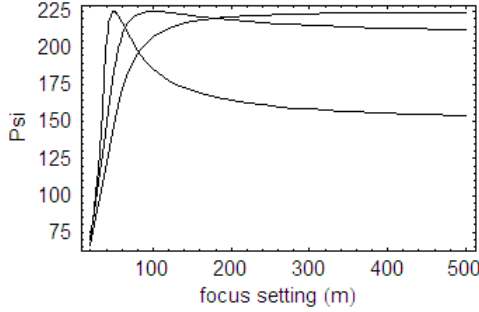


Figure 6 Plot of normalised axial image intensity versus focus setting. The three curves correspond to point source targets at ranges 50m, 100m and 10km

Sensitivity analysis

The sensitivity depends on the relative contributions of signal and noise in (7). Noise contributions could be minimised by using an appropriately designed heterodyne signal processing chain as shown in Figure 7. This contains an IF filter to limit shot noise and a baseband filter to limit speckle noise. The noise term ϕ_n in (3) has a speckle bandwidth considerably higher than the acoustic fluctuations. The IF filter needs to be sufficiently broad to encompass the speckle fluctuations while the baseband filter is selected to pass the acoustic frequencies of interest.

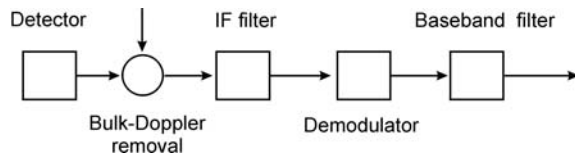


Figure 7 Typical signal processing chain in a laser radar heterodyne receiver.

The synthetic image signal to noise ratio will depend on the increase $\Delta\Psi$ due to the presence of a signal compared with the standard deviation in Ψ from measurement to measurement, σ_Ψ . Calculations lead to

$$\frac{\Delta\Psi}{\sigma_\Psi} = \frac{N-1}{\sqrt{2} \left(1 + \frac{\langle \phi_n^2 \rangle}{N_s \langle \phi_s^2 \rangle} \right) \sqrt{\frac{\pi}{\beta T} \operatorname{erf}(\beta T) - \frac{1}{(\beta T)^2} (1 - \exp(-(\beta T)^2))}} \quad (15)$$

where $\langle \phi_s^2 \rangle = 4k^2 p_{rms}^2 / Z^2$, β is the bandwidth of the baseband filter and N_s is the number of speckles sampled per array element. N_s can be greater than 1 if multiple detectors are used per beam arranged side-by-side in the receiver plane. The effect of temporal integration has been included, with T being the integration time. For the case of large arrays, sufficiently long integration times, and weak acoustic signals, (15) simplifies to

$$\frac{\Delta\Psi}{\sigma_\Psi} \approx G \times \frac{\langle \phi_s^2 \rangle}{\langle \phi_n^2 \rangle} \quad (16)$$

where $G = NN_s \sqrt{\beta T} / \sqrt{2\pi}^{1/4}$. G represents the gain of the phased array while $\langle \phi_s^2 \rangle / \langle \phi_n^2 \rangle$ is the signal to noise ratio of a single channel in isolation. G is proportional to the total number of speckles sampled, the square root of the bandwidth and the square-root of the integration time. This could potentially be a very large gain factor, e.g. for a 4-beam system with 20 range gates and 19 speckles per beam, a bandwidth of 300Hz and an integration time of 1s, then $G = 26,000$ (i.e. the phased array could detect a signal 26,000 times weaker than a single detector with no averaging).

The minimum detectable signal (noise floor) can be calculated by setting $\Delta\Psi / \sigma_\Psi = 1$ leading to

$$L_{p,\min} = 10 \log \left\{ \frac{\sqrt{2\pi}^{1/4} Z^2 \omega_s^2}{4k^2 \langle \cos^2(\theta) \rangle p_{ref}^2 N_s (N-1) \sqrt{\beta T}} \frac{\langle \phi_n^2 \rangle}{\langle \phi_s^2 \rangle} \right\} \quad (17)$$

Calculations of phase noise in a heterodyne receiver, $\langle \phi_n^2 \rangle$ are performed using the methods described in References 4 and 5. Figure 8 gives results for a baseband filter band-pass from 300 to 600Hz, and assuming the heterodyne carrier to noise ratio is sufficiently strong that shot noise can be neglected.

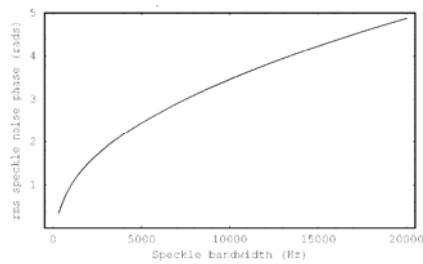


Figure 8 Calculated rms speckle noise after baseband filter versus speckle bandwidth.

A typical speckle bandwidth is estimated to be 10 kHz giving a rms phase noise per detector of 3 rad. An underwater array would benefit from relatively high levels of backscatter and might use 4 beams with 40 range gates per beam and 19 speckles sampled per range gate. With these parameters and 1s averaging, the estimated sensitivity from (17) is 128 dB Re 1 μ Pa. An atmospheric sensor might use 19 beams with only 1 speckle and range bin per beam if the backscatter is weak. The sensitivity from (17) with 1s averaging is 64 dB Re 20 μ Pa. The sensitivity is indicated by the dotted line in Figure 2 and corresponds in both cases to the volume of speech at 1m range. Sources to the right of the line, including vehicles and hostile fire are detectable.

Conclusions

It has been shown theoretically that acoustic images can be synthesised from multi-beam LIDAR data. An array of virtual microphones is projected into the medium and the array is steered in processing to build up 2 or 3-dimensional representations of the scene. System gain varies with the number of elements and angular resolution

is determined by the size of the array. While the aperture and resolution may be very high in the air environment, the sensitivity is poorer than would be obtained with conventional microphones or the human auditory system. Nevertheless the technique offers high resolution detection of relatively loud sources in adverse conditions where conventional optical imaging techniques may fail, and the useful capability of detecting and locating objects in hide or beyond line-of-sight.

References

1. Wikipedia article, "Sound Pressure", http://en.wikipedia.org/wiki/Sound_pressure.
2. Internet article, "Science of Sound in the Sea", <http://www.dosits.org/science/ssea/2.htm>.
3. Hecht and Zajac, "Optics", Addison-Wesley (1974).
4. K.D. Ridley and E. Jakeman, "FM demodulation in the presence of multiplicative and additive noise", *Inverse Problems*, vol. 15, p989 (1999).
5. K.D. Ridley and E. Jakeman, "Signal to noise analysis of FM demodulation in the presence of multiplicative and additive noise", *Signal Processing*, vol. 80, p1895 (2000).

Acknowledgements

The work reported in this paper was funded by the Electro-magnetic Remote Sensing (EMRS) Defence Technology Centre, established by the UK Ministry of Defence and run by a consortium of SELEX Galileo, Thales UK and Roke Manor Research.